Journal of Medicinal Chemistry Article

J. Med. Chem. **2010,** *53,* 139–146 **139**
DOI: 10.1021/jm900803q

In Vivo Positron Emission Tomography (PET) Imaging of Mesenchymal−Epithelial Transition (MET) Receptor

Chunying Wu,[†] Zhe Tang,[‡] Weiwen Fan,[‡] Wenxia Zhu,[†] Changning Wang,[†] Edurado Somoza,[†] Norbert Owino,[†] Ruoshi Li,[†] Patrick C. Ma,[‡] and Yanming Wang*,[†]

[†]*Division of Radiopharmaceutical Science, Case Center for Imaging Research, Department of Radiology, Case Western Reserve University, Cleveland, Ohio 44106 and* [‡]*Division of Hematology/Oncology, Department of Medicine, Case Western Reserve University, University Hospitals Case Medical Center, and Case Comprehensive Cancer Center, Cleveland, Ohio 44106*

Received June 4, 2009

We report the radiosynthesis and evaluation of 3-[3,5-dimethyl-4-(4-[^{11}C]methylpiperazinecarbonyl)-1*H*-pyrrol-2-ylmethylene]-2-oxo-2,3-dihydro-1*H*-indole-5-sulfonic acid (3-chlorophenyl)methylamide, termed [^{11}C]SU11274 ([^{11}C]**14**) for in vivo imaging of mesenchymal−epithelial transition (MET) receptor by positron emission tomography (PET). Following the synthesis of the precursor (**13**) that was achieved in 10 steps with a total yield of 9.7%, [^{11}C]**14** was obtained through radiomethylation in a range of 5−10% radiochemical yield and over 95% radiochemical purity. For in vivo PET studies, two human lung cancer xenograft models were established using MET-positive NCI-H1975 and MET-negative NCI-H520 cell lines. Quantitative [^{11}C]**14**-PET studies showed that the tumor uptake of [^{11}C]**14** in the NCI-H1975 xenografts was significantly higher than that in the NCI-H520 xenografts, which is consistent with their corresponding immunohistochemical tissue staining patterns of MET receptors from the same animals. These studies demonstrated that [^{11}C]**14**-PET is an appropriate imaging marker for quantification of MET receptor in vivo, which can facilitate efficacy evaluation in the clinical development of MET-targeted cancer therapeutics.

1. Introduction

Cancer therapy for humans has entered into a new era of molecular medicine.[1] To date, a series of small molecule inhibitors such as imatinib,[2] gefitinib, erlotinib, lapatinib,[3] sunitinib,[4] and sorafenib[5] have been approved by the U.S. Food and Drug Administration for cancer therapies that target various receptor tyrosine kinases (RTKs[a]). An important RTK that plays a prominent role in regulating invasive cellular oncogenic signaling is mesenchymal−epithelial transition (MET) receptor.[6,7] Upon binding of its natural ligand hepatocyte growth factor/scatter factor, MET is phosphorylated at a number of juxtamembrane and cytoplasmic kinase phosphoepitopes, resulting in signal transduction and regulation of multitudes of cellular mitogenic and motogenic processes such as cell growth, proliferation, and survival.[6,8,9] Overexpression or mutation of MET results in activation of oncogenic signaling pathways and leads to up-regulation of diverse tumor cell functions.[7,10] Mounting evidence has validated MET receptor as a novel target for anticancer therapy.[11−17]

For efficacy evaluation of various MET-targeted anticancer therapies currently under development, it is critical to develop an imaging tool that permits detection and quantification of MET expression in vivo. Although invasive biopsy provides spatially and temporally static information about the expression of MET, it is often not feasible in clinical trials, especially in lung tumors. Therefore, there is an urgent need to develop noninvasive molecular imaging techniques to assay and quantify the putative molecular targets such as MET in human subjects. For this reason, several imaging modalities have been explored for in vivo imaging of MET expression. Magnetic resonance imaging (MRI) together with Doppler ultrasound were first used to measure blood oxygenation level, which was found to correlate with MET activity in vivo.[18,19] An anti-MET contrast agent was also evaluated on the basis of a superparamagnetic iron oxide for MRI imaging of MET expression.[20] In addition, PET and single photon emission computed tomography (SPECT) were used in combination with anti-Met monoclonal antibodies that were radiolabeled with either zirconium-89 for PET or iodine-125 for SPECT.[21,22]

To date, several small molecule MET inhibitors have been developed.[11,17,23−34] Among them, 3-[3,5-dimethyl-4-(4-[^{11}C]-methylpiperazinecarbonyl)-1*H*-pyrrol-2-ylmethylene]-2-oxo-2,3-dihydro-1*H*-indole-5-sulfonic acid (3-chlorophenyl)-methylamide, **14** (SU11274), is a specific, reversible MET inhibitor that induces apoptosis in cells transformed by oncogenic MET and translocated promoter region-MET tyrosine kinase.[11] Compound **14** inhibits the catalytic activity of MET with an IC_{50} of 20 nM and a selectivity at least 1 order of magnitude higher than that for a variety of other tyrosine kinases.[11,35] Inhibition of the MET kinase activity by **14** leads to time- and dose-dependent reduction of cell growth by inducing G1 cell cycle arrest and apoptosis. In addition, **14** possesses a structure that permits direct radiolabeling with

*To whom correspondence should be addressed. Phone: +1-216-844-3288. Fax: +1-216-844-8062. E-mail: yanming.wang@case.edu.

[a] Abbreviations: EGFR, epidermal growth factor receptor; MET, mesenchymal−epithelial transition; MRI, magnetic resonance imaging; PET, positron emission tomography; RTK, receptor tyrosine kinases; SMP, small-molecule probe; SPECT, single photon emission computed tomography.

Published on Web 12/07/2009

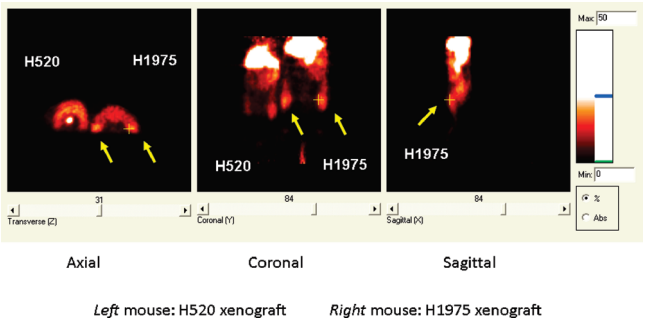

Figure 1. [^{11}C]**14**-PET imaging of lung cancer xenografts. Coronal micro-PET images of nude mouse pair xenografted with NCI-H520 (animal on the left) and NCI-H1975 (animal on the right). Mice were injected with 18.5 MBq of [^{11}C]**14** via the tail vein, and dynamic scanning was performed for 90 min thereafter as detailed in the Experimental Section. Image planes have been chosen for illustration where both the left and right tumors are visible. The locations of the lung cancer tumor xenografts are highlighted by yellow arrows.

positron-emitting carbon-11 that will not cause any alternation of the authentic structure. Thus, the binding properties and pharmacokinetics of **14** will be preserved. These binding affinity and specificity as well as its flexibility for radiolabeling make **14** a promising small-molecule probe (SMP) for PET imaging of MET expression. Compared to immuno-PET imaging, SMP-PET imaging holds several advantages: (1) SMPs can be directly radiolabeled with a clearly defined structure so that the pharmacokinetics, toxicity, and metabolism can be precisely determined; (2) SMP PET provides a more quantitative capacity than immuno-PET; (3) the structures of SMP can be readily modified for optimal imaging outcomes. In this study we report the first multistep synthetic approach to the production of [^{11}C]**14**. We also investigated the potential of [^{11}C]**14** for PET imaging of MET expression in vivo in human lung cancer xenografts (Figure 1).

2. Results

2.1. Synthesis of the Labeling Precursor. The synthesis of the [^{11}C]**14** labeling precursor is described in Scheme 1. The 2-oxo-2,3-dihydro-1*H*-indole-5-sulfonic acid (**3**) was first prepared starting from the commercially available 1,3-dihydroindolin-2-one (**1**). Sulfonation of **1** yielded 2-oxo-2,3-dihydro-1*H*-indole-5-sulfonic acid (**2**), which underwent amidation of the sulfonyl chloride group to yield the indole sulfonamide (**3**).[36,37] The oxime (**5**) was then prepared from *tert*-butyl acetoacetate (**4**) based on previously reported procedures.[38,39] Knorr reaction of **5** with ethyl 3-oxobutyrate (**6**) in the presence of zinc dust gave 3,5-dimethyl-1*H*-pyrrole-2,4-dicarboxylic acid 2-*tert*-butyl ester 4-ethyl ester (**7**) in quantitative yield. The decarboxylation of the pyrrole **7** under acidic conditions (hydrochloric acid/ethanol) yielded 2,4-dimethyl-1*H*-pyrrole-3-carboxylic acid ethyl ester (**8**), which underwent Vilsmeier formylation to give the key intermediate 5-formyl-2,4-dimethyl-1*H*-pyrrole-3-carboxylic acid ethyl ether (**9**) for the aldol condensation of the oxindole and pyrrole aldehyde moieties. Basic hydrolysis of **9** yielded 5-formyl-2,4-dimethyl-1*H*-pyrrole-3-carboxylic acid (**10**). Amidation of **10** with piperazine-1-carboxylic acid *tert*-butyl ester in the presence of 1-(3-dimethylaminopropyl)-3-ethylcarbodiimide hydrochloride and hydroxybenzotriazole yielded the functionalized pyrrole aldehyde 4-(5-formyl-2,4-dimethyl-1*H*-pyrrole-3-carbony)piperazine-1-carboxylic acid *tert*-butyl ester (**11**). Coupling of the pyrrole aldehyde **11** and oxindole sulfonamide **3** in the presence of pyrrolidine yielded 4-(5-{5-[3-chlorophenyl)-methyl sulfomyl]-2-oxodihydroindol-3-yllidenemethyl}-2,4-dimethyl-1*H*-pyrrole-3-carbonyl)piperazine-1-carboxylic acid tert-butyl ester (**12**). Further decarboxylation of **12** with hydrochloric acid in ethyl acetate afforded the precursor 3-[3,5-dimethyl-4-(piperazine-1-carbonyl)-1*H*-pyrrol-2-yl-methylene]-2-oxo-2,3-dihyro-1*H*-indole-5-sulfonic acid (3-chlorophenyl)methylamide hydrochloride (**13**) for ^{11}C radiolabeling of **14**.[40,41]

2.2. Radiosynthesis of [^{11}C]14. The radiosynthesis of [^{11}C]**14** was accomplished through direct methylation of **13** with [^{11}C]methyl iodide in the presence of potassium carbonate (see Scheme 2). After reaction for 10 min at 140 °C, the resulting mixture was subjected to a purification procedure using solid-phase extraction on C-18 Sep-Pak cartridge prior to semipreparative HPLC purification. The overall radiochemical yield of [^{11}C]**14** was 5−10% decay corrected to the activity of [^{11}C]methyl iodide trapped. [^{11}C]**14** was obtained with radiochemical purity of over 98% and a specific activity of 0.3−0.5 Ci/mmol at the end of synthesis. The radiochemical identity of [^{11}C]**14** was verified by co-injection with the nonradioactive cold standard which was commercially purchased from Sigma-Aldrich (St. Louis, MO).

2.3. Preparation of Human Lung Cancer Xenografts and in Vivo Micro-PET/MRI Studies. For in vivo imaging studies, murine xenograft tumor models were established from two different human lung cancer cell lines, NCI-H1975 (high MET expression) and NCI-H520 (negligible MET expression).[42] The human lung cancer xenografts were established as described in the Experimental Section. For each imaging study, a pair of mice was used and placed on the same bed under anesthesia. After initial localization scans, [^{11}C]**14** (500 μCi, 18.5 MBq) was then administrated through tail vein injection into each of the two mice. Dynamic micro-PET imaging was performed immediately for 90 min of duration. The mice were kept on the same bed and transferred to the 9.4 T MRI scanner. T2-weighted MRI images were acquired for 30 min. Following micro-PET and MRI scans, images from both modalities were coregistered for quantitative measurements of [^{11}C]**14** concentration in each of the tumor regions. The radioactivity concentrations were determined as standard uptake value (SUV) in each region of interest through 90 min of the PET scan (Figure 2).

2.4. Correlation of MET Expression by ex Vivo Bioassay. Following imaging studies, the tumor tissues were harvested for immunohistochemical staining for correlation with the [^{11}C]**14**-PET imaging results. Thus, immunoblotting and the respective H&E staining of both tumor xenografts were first conducted for comparison of MET expression. As shown in Figure 3, NCI-H1975 cells express high levels of both MET and epidermal growth factor receptor (EGFR), which are phosphorylated under serum-stimulated conditions. On the other hand, NCI-H520 expresses negligible levels of MET and EGFR. The two cell lines were used to establish tumor xenografts in nude mice. In addition, immunohistochemical analysis of MET expression was conducted (Figure 4). In NCI-H520 xenograft, negligible MET expression was observed (0 to 1+) (Figure 4a,b). On the other hand, MET expression was seen at a much higher level (3+) in the NCI-H1975 xenograft (Figure 4c,d), and significant membranous localization of the MET staining is evident in this cell line as well (Figure 4d, yellow arrows). These results are in concordance with the cell line expression data under cell culture conditions.

Scheme 1. Synthesis of the ^{11}C Radiolabeling Precursor **13**

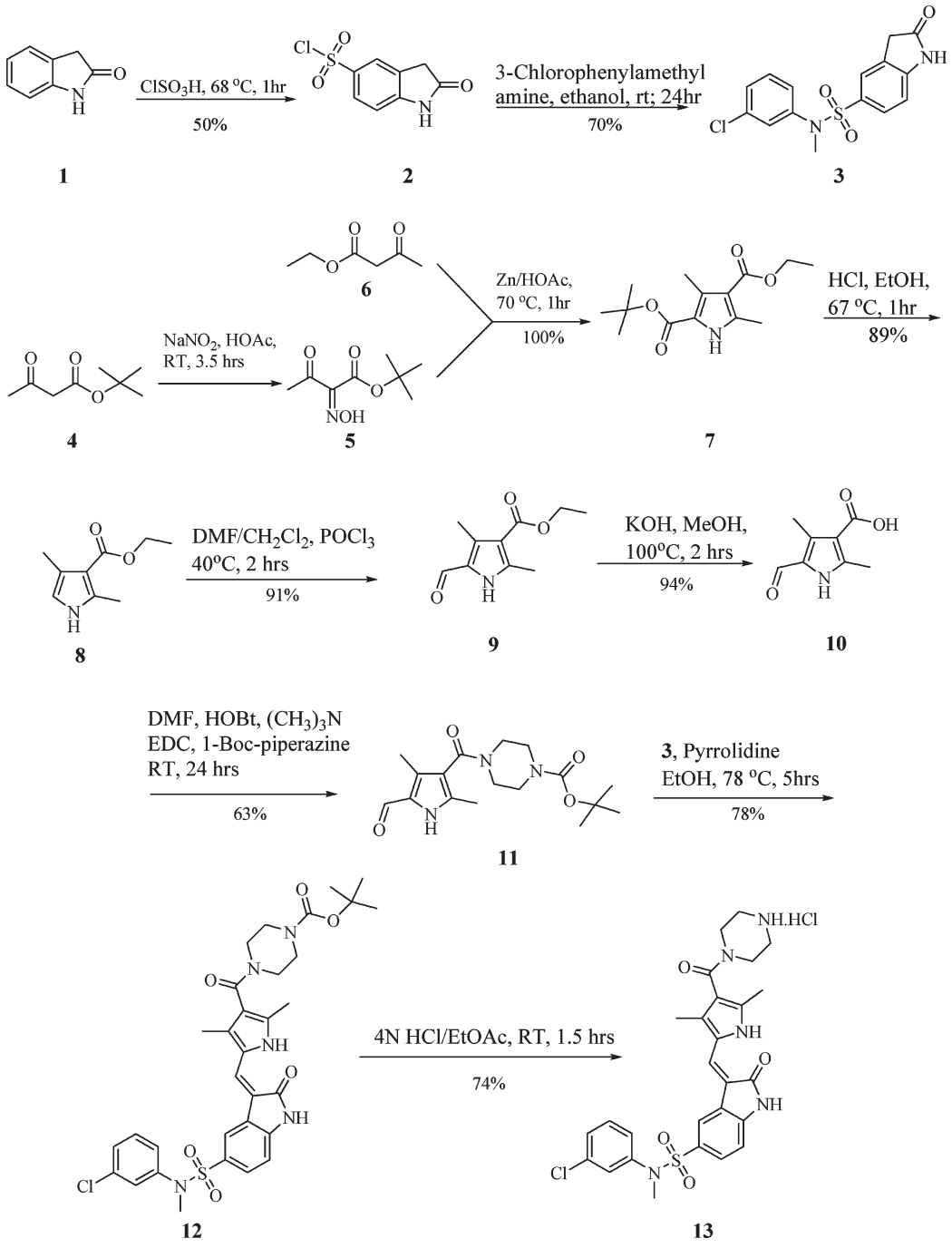

3. Discussion

As a linear compound, **14** consists of three functionalized heterocyclic components: oxindole, pyrrole, and piperazine. The methyl group on the nucleophilic nitrogen of the piperazine ring is uniquely suited as a radiolabeling site. This is due to the fact that the *N*-methyl group can be readily replaced by a [^{11}C]methyl group through direct radiomethylation with [^{11}C]methyl iodide without causing any structural alternation. For this reason, we designed **13** with no methyl group on the piperazine ring as the radiolabeling precursor, which is otherwise identical to **14**, the final product. Because of this structural variation, the chemical synthesis of **13** warrants design of a new synthetic approach that is different from the previously reported approach to **14**. The synthetic approach we have developed consists of the following three steps: (1) preparation of the oxindole core; (2) preparation of functionalized pyrrole aldehyde unit; (3) aldol condensation of the oxindole and pyrrole aldehyde units to furnish the indolinone.[36] Starting from commercially available 2-oxindole, the total synthesis of **13** was achieved in 10 steps with a combined yield of 9.7%. By use of this synthetic route, large quantities of **13** can be obtained, which can be stored as the HCl salt for long periods without decomposition.

The radiosynthesis of [^{11}C]**14** was achieved through direct radiomethylation using [^{11}C]methyl iodide, which was prepared through reduction of [^{11}C]CO_2 generated by an on-site cyclotron. Although there are a total of five nitrogens present in **13**, only the unsubstituted nitrogen in the unconjugated piperazine

Scheme 2. Radiosynthesis of [^{11}C]**14**

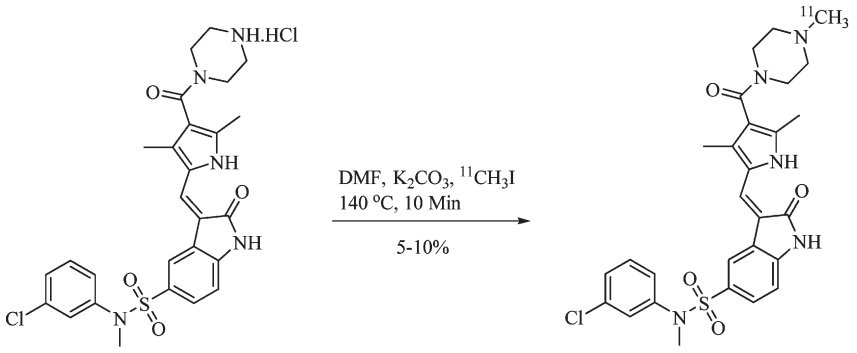

13 **[^{11}C] SU11274 ([^{11}C]14)**

ring can be methylated by [^{11}C]methyl iodide in the presence of potassium carbonate. The radiomethylation was carried out at elevated temperature (140 °C) in DMF for 10 min. The [^{11}C]**14** product was purified by HPLC with a radiochemical purity of >95% and a radiochemical yield of 5−10% after decay correction.

The in vivo imaging studies were carried out in two lung cancer xenograft mouse models, which were prepared with NCI-H520 and NCI-H1975 lung adenocarcinama cells. H1975 cells express high level of wild-type MET without genomic amplification. In contrast, MET expression in H520 cells is negligible. Thus, use of both xenografts allowed us to determine the specificity of [^{11}C]**14**-PET imaging in vivo. As shown in Figure 2, time−radioactivity curves were determined in both xenograft tumor models, which showed that the uptake of the [^{11}C]**14** in the NCI-H1975 xenograft was significantly higher than in the NCI-H520 xenograft (p = 0.000 19). Compared to NCI-H520 xenograft mice, the NCI-H1975 xenograft mice exhibited an increased tumor uptake of [^{11}C]**14** throughout the entire measurement period of 90 min. At 10 min postinjection of [^{11}C]**14**, the radioactivity concentration in NCI-H1975 mice was 1.35-fold higher than that in NCI-H520 mice. Moreover, at 65 min postinjection, the radioactivity concentration ratio of H1975/H520 reached a statistically significant and enhanced ratio of 2.1 and peaked at 2.6 at 80 min postinjection. Hence, our results suggest that [^{11}C]**14**-PET is a specific imaging marker that can differentiate and quantify MET expression in vivo.

Immediately following completion of the micro-PET imaging, the tumor xenografts were dissected and MET expression in tumor tissues of both xenograft mouse models was evaluated through immunoblotting and immunohistochemical staining using antihuman MET antibody (Figures 3 and 4). The results confirmed that NCI-H1975 xenograft tumor cells expressed a readily detectable high level of MET receptor, with both membranous and cytoplasm localization discernible through standard immunohistochemistry using antihuman MET antibody. On the other hand, NCI-H520 xenograft tumor cells showed negligible MET expression level and specifically no membranous MET localization was seen. These results are consistent with the imaging data and thus demonstrate that [^{11}C]**14**-PET is a promising imaging marker of MET expression.

In summary, we successfully developed an efficient radiochemical synthesis of [^{11}C]**14**. Micro-PET studies demonstrated that the tumor uptake of [^{11}C]**14** is consistent with the levels of MET expression in the xenograft tumor models. The [^{11}C]**14**-PET imaging results correlated well with the MET immunohistochemistry bioassay results, suggesting that [^{11}C]**14**-PET is a valid imaging marker for in vivo quantification of MET expression. These results justify further development of [^{11}C]**14** and its analogues as molecular imaging probes for efficacy evaluation of MET-targeted cancer therapy.

4. Experimental Section

4.1. General Remarkers. All chemicals were purchased from Sigma-Aldrich (St. Louis, MO) and used without further purification unless otherwise specified. ^{1}H NMR spectra were recorded on a Bruker AMX 400 MHz spectrometer using 5 mm NMR tubes (Wilmad 528-PP) in $CDCl_3$ or DMSO-d_6 (Sigma-Aldrich or Cambridge Isotopes) solutions at room temperature. Chemical shifts are reported as δ values relative to internal tetramethylsilane (TMS). HR-ESIMS were recorded under the electron spray ionization (ESI) condition. ^{13}C NMR spectra were recorded on an Oxford AS 100 MHz spectrometer using 5 mm NMR tubes (Wilmad 528-PP) in $CDCl_3$ or DMSO-d_6 (Sigma-Aldrich or Cambridge Isotopes). Six-week-old female Ncr-nu (Nude) mice were purchased from Charles River Laboratories (Wilmington, MA) and hosted in a pathogen-free animal facility at Case Western Reserve University, Cleveland, OH. Analytical radio-TLC was performed on silica gel F-254 aluminum plates, with visualization under UV (254 nm). Chemical and radiochemical purity was determined by an Agilent 1100 series high pressure liquid chromatography (HPLC) system equipped with UV and Bioscan flow count detectors. The purities of all the intermediates and final product were >95%. Micro-PET imaging was conducted under an R4 micro-PET system (Siemens Medical Solutions, Knoxville, TN). MRI imaging was performed on a Bruker Biospec 9.4 T MRI scanner to produce high resolution images as roadmaps for micro-PET imaging.

4.2. Synthesis of 2-Oxo-2,3-dihydro-1*H*-indole-5-sulfonic Acid (2). Chlorosulfonic acid (27 mL, 406 mmol) was slowly added to a solution of 1,3 dihydroindolin-2-one (**1**, 13.3 g, 100 mmol) at room temperature. The reaction mixture was stirred at room temperature for 1.5 h followed by stirring for another 1 h at 68 °C in a water bath. The reaction mixture was then cooled to room temperature and poured into water. The solid precipitate was filtered, washed with water, and dried to yield 2-oxo-2,3-dihydro-1*H*-indole-5-sulfonic acid (**2**, 11.0 g, 50% yield), which was used without further purification.

4.3. Synthesis of 2-Oxo-2,3-dihydro-1*H*-indole-5-sulfonic Acid (3). To a solution of compound **2** (4.2 g, 18.2 mmol) dissolved in dry ethanol (10 mL), 3-chlorophenylamine (3.0 g, 21 mmol) was added. The resulting solution was stirred at room temperature for 12 h. The reaction mixture was then concentrated and recrystallized from dichloromethane to give 2-oxo-2,3-dihydro-1*H*-indole-5-sulfonic acid (**3**, 4.3 g 70% yield). ^{1}H NMR (400 MHz, DMSO-d_6): 10.89 (br, s, NH), 6.92−7.16 (m, 7H, aromatic H), 3.53 (s, 2H, CH_2), 3.08 (s, 3H, CH_3).

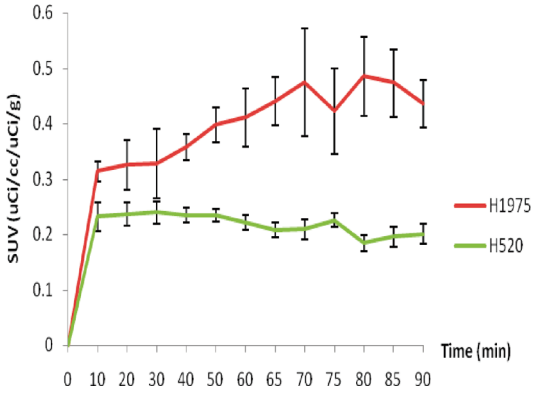

Figure 2. Pharmacokinetic profile of [^{11}C]**14**-PET imaging of lung cancer xenografts. The average radioactivity−time curve in terms of SUV during the time period of [^{11}C]**14**-PET imaging of each of the lung cancer xenografts was plotted as illustrated. The radiotracer uptake level in NCI-H1975 xenograft is higher than that in the control xenograft NCI-H520 (p = 0.000 19). Regions of interest were manually drawn by creating a volume of interest in the tumor region based on MR images. $p < 0.05$ indicates statistical significance.

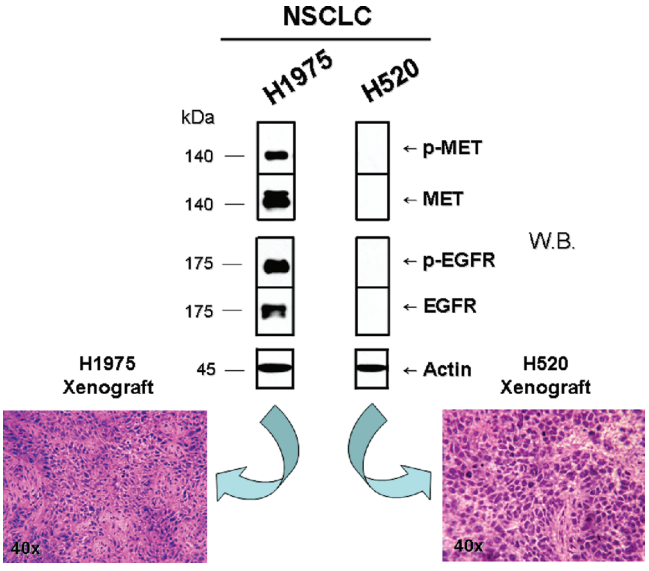

Figure 3. Murine xenograft models of human NCI-H1975 and NCI-H520 lung cancer cell lines. Expression of MET and EGFR in the NCI-H1975 and NCI-H520 human lung cancer cell lines is shown here. The two lung cancer cell lines were cultured in regular growth media in cell culture, with the cell lysates collected for SDS−PAGE and immunoblotting using phospho-MET and total MET antibodies as described in the Experimental Section. Immunoblotting using antiphospho-EGFR and anti-EGFR antibodies was also performed for comparison. Actin antibody was used as a protein loading control. H&E staining of the xenografts is also shown here (40X).

4.4. Synthesis of *tert*-Butyl 2-Hydroximino-3-oxobutyrate (5). *tert*-Butyl 3-oxobutanoate (40 mL, 241 mmol) was dissolved in acetic acid (80 mL) in a round-bottomed flask, and the mixture was cooled in an ice bath to about 10 °C. Sodium nitrite (18 g, 261 mmol) was added over 1 h while keeping the temperature under 15 °C. The cold bath was removed and the mixture was allowed to stir for 3.5 h at room temperature to give a crude solution of *tert*-butyl 2-hydroximino-3-oxobutyrate (**5**) which was used in the next step without further purification.

4.5. Synthesis of 3,5-Dimethyl-1*H*-pyrrole-2,4-dicarboxylic Acid 2-*tert*-Butyl Ester 4-Ethyl Ester (7). To a stirred mixture of ethyl 3-oxobutyrate (**6**, 10 mL, 79 mmol) and acetic acid

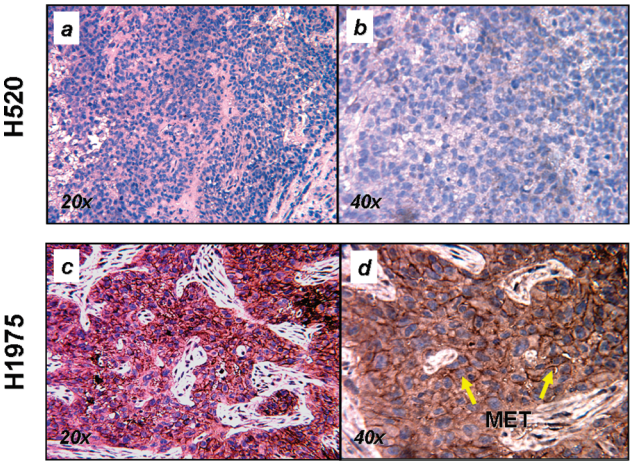

Figure 4. Immunohistochemical analysis of MET receptor expression in tumor xenograft of human lung cancer (NCI-H1975 and H520) in vivo. The expression of MET receptor in the lung cancer xenografts established was evaluated using immunohistochemistry of the xenograft formalin-fixed paraffin-embedded sections using anti-MET primary antibody as described in the Experimental Section.

(100 mL) in an oil bath, zinc dust (50 g 0.76 mol) was added portionwise. The mixture was heated to 60 °C. At this temperature, the crude *tert*-butyl 2-hydroximinooxobutyrate precipitated slowly. The temperature was then increased to 75 °C for 1 h, and then the reaction mixture was poured into water (40 mL). The precipitate was collected by filtration to yield 3,5-dimethyl-1*H*-pyrrole-2,4-dicarboxylic acid 2-*tert*-butyl ester-4-ethyl ester (**7**) in quantitative yield as a white solid. ^{1}H NMR (400 MHz, $CDCl_3$): 9.47 (br, s, 1H, NH), 4.29 (q, 2H, CH_2), 2.52, 2.54 (2s, 6H, $2CH_3$), 1.58 (s, 9H, $3CH_3$), 1.36 (t, 3H, CH_3). ^{13}C NMR (100 MHz, CD_3SO): 165.8, 161.6, 138.7, 130.2, 119.4, 113.6, 81.4, 59.6, 28.7, 14.7, 14.6, 12.3. Retention time: 5.98 min (HPLC C-18 column, acetonitrile/DMGA (5 mM, pH 7.4) = 80:20 (v:v)).

4.6. Synthesis of 2,4-Dimethyl-1*H*-pyrrole-3-carboxylic Acid Ester (8). A solution of the product **7** (18 g, 67 mmol) dissolved in ethanol (78 mL) was stirred vigorously as hydrochloric acid (10 N, 3.6 mL) was slowly added at 20 °C. Then the reaction mixture was heated to 67 °C for 1 h, cooled to 5 °C, and poured into ice water. The solid was collected by filtration and washed with water to yield 2,4-dimethyl-1*H*-pyrrole-3-carboxylic acid ester (**8**, 10 g, 89% yield). ^{1}H NMR (400 MHz, $CDCl_3$): 10.48 (br, s, 1H, NH), 6.35 (s, 1H, CH), 4.10 (q, 2H, CH_2), 2.35, 2.15 (2s, $2CH_3$), 1.21 (t, 3H, CH_3). ^{13}C NMR (100 MHz, DMSO-d_6): 166.0, 135.9, 120.1, 115.4, 110.2, 58.9, 15.1, 14.2, 13.3. Retention time: 3.42 min (HPLC C-18 column, acetonitrile/DMGA (5 mM, pH 7.4) = 80:20 (v:v), flow rate 1.0 mL/min).

4.7. Synthesis of 5-Formyl-2,4-dimethyl-1*H*-pyrrole-3-carboxylic Acid Ethyl Ester (9). Phosphorus oxychloride (2.8 mL, 30 mmol) was added dropwise to a solution of dimethylformamide (2.3 mL, 30 mmol) in dry dichloromethane (50 mL) in an ice bath. After 30 min compound **8** (3.5 g, 21 mmol) was slowly added. The mixture was heated at 40 °C for 2 h, cooled to 10 °C, followed by addition of ice−water (10 mL) and hydrochloric acid (10 N, 10 mL) with vigorous stirring. The mixture was allowed to stand at room temperature for 12 h until the layers were separated. The aqueous layer was adjusted to pH 12−13 with potassium hydroxide (10 N), while the temperature was maintained at 55 °C. The reaction mixture was then cooled to 10 °C in an ice bath and stirred for another hour. The solid formed was collected by filtration and washed with water to yield 5-formyl-2,4-dimethyl-1*H*-pyrrole-3-carboxylic acid ethyl ester (**9**, 3.7 g, 91%). ^{1}H NMR (400 MHz, $CDCl_3$): 10.79 (s, 1H, NH), 9.60 (s, 1H, CHO), 4.31 (q, 2H, CH_2), 2.56, 2.60

(2s, $2CH_3$), 1.38 (t, 3H, CH_3). ^{13}C NMR (100 MHz, DMSO-d_6): 177.6, 165.3, 144.4, 136.9, 128.5, 114.4, 59.9, 14.6, 14.5, 10.9. Retention time: 3.35 min (HPLC C-18 column, acetonitrile/DMGA (5 mM, pH 7.4) = 80:20 (v:v), flow rate 1.0 mL/min).

4.8. Synthesis of 5-Formyl-2,4-dimethyl-1*H*-pyrrole-3-carboxylic Acid (10). A mixture of compound **9** (3.0 g, 15.4 mmol), potassium hydroxide pellet (1.2 g, 16.5 mmol), methanol (8 mL), and water (50 mL) was heated at 100 °C for 2 h and subsequently cooled to 8 °C in an ice bath. The reaction product was extracted with dichloromethane. The aqueous portion was acidified to pH 4 with hydrochloric acid (10 N). The product was collected by filtration, washed with water, and dried over $MgSO_4$ to yield 5-formyl-2,4-dimethyl-1*H*-pyrrole-3-carboxylic acid (**10**, 2.4 g, 94% yield) as a yellow solid. ^{1}H NMR (400 MHz, DMSO-d_6): 12.07 (s, 1H, NH), 9.60 (s, 1H, CHO), 3.33 (s, 1H, COOH), 2.39, δ 2.43 (2s, $2CH_3$). ^{13}C NMR (100 MHz, DMSO-d_6): 178.4, 166.6, 143.4, 134.7, 128.8, 114.0, 14.3, 11.1. Retention time: 2.33 min (HPLC, C-18 column, acetonitrile/DMGA (5 mM, pH 7.4) = 80:20 (v:v), flow rate 1.0 mL/min).

4.9. Synthesis of 4-(5-Formyl-2,4-dimethyl-1*H*-pyrrole-3-carbonyl)piperazine-1-carboxylic Acid *tert*-Butyl Ester (11). A solution of compound **10** (2.0 g, 12 mmol) dissolved in dimethylformamide (40 mL) was stirred at room temperature while *N*-(3-dimethylaminopropyl)-*N*-ethylcarbodiimide hydrochloride (3.5 g, 18 mmol), hydroxybenzotriazole hydrate (2.4 g, 18 mmol), triethylamine (15 mL), and 1-Boc-piperazine (2.8 g, 15 mmol) were added. The reaction mixture was stirred at room temperature for 12 h and then diluted with water (30 mL), brine (20 mL), saturated sodium carbonate (30 mL). The pH of the resultant mixture was adjusted to 10 with sodium hydroxide (10 N) and extracted with 10% methanol in dichloromethane. The organic extract was dried over anhydrous sodium sulfate and rotary-evaporated to dryness. The dry product was treated with toluene (19 mL) and rotary-evaporated again to dryness. The residue was triturated with hexane/diethyl ether, 3:1 v/v (15 mL), then washed with ethyl acetate to give 4-(5-formyl-2,4-dimethyl-1*H*-pyrrole-3-carbonyl)piperazine-1-carboxylic acid *tert*-butyl ester (**11**, 2.5 g, 63%). ^{1}H NMR (400 MHz, $CDCl_3$): 11.86 (s, 1H, NH), 9.48 (s, 1H, CHO), 3.30 (br, s, 8H, piperazy ring), 2.18, 2.13 (2s, $2CH_3$), 1.36 (s, 9H, $3CH_3$). ^{13}C NMR (150 MHz, CD_3SO): 177.8, 166.0, 161.7, 154.4, 136.4, 128.6, 119.3, 79.8, 45.2, 28.6, 21.9, 12.4, 9.9. Retention time: 2.92 min (HPLC C-18 column, acetonitrile/DMGA (5 mM, pH 7.4) = 80:20 (v:v), flow rate 1.0 mL/min).

4.10. Synthesis of 4-(5-{5-[3-Chlorophenyl)methylsulfomyl]-2-oxodihydroindol-3-yllidenemethyl}-2,4-dimethyl-1*H*-pyrrole-3-carbonyl)piperazine-1-carboxylic Acid *tert*-Butyl Ester (12). A mixture of compounds **3** (1.0 g, 2.9 mmol) and **11** (1.2 g, 3.6 mmol) and pyrrolidine (3 mL) was dissolved in ethanol and heated to 90 °C for 5 h. After the reaction mixture was cooled to room temperature, the precipitate was filtered, washed with ethanol, and dried to yield 4-(5-{5-[3-chlorophenyl)methylsulfomyl]-2-oxodihydroindol-3-yllidenemethyl}-2,4-dimethyl-1*H*-pyrrole-3-carbonyl)piperazine-1-carboxylic acid *tert*-butyl ester (**12**, 1.5 g, 78% yield). ^{1}H NMR (400 MHz, DMSO): δ 7.65−6.95 (m, 7H, aromatic-H and 1H, olefinic-H), 3.30 (m, 8H, piperazyl-H), 3.15 (s, 3H, CH_3), 2.29, 2.35 (2s, $2CH_3$), 1.47 (s, 9H, $3CH_3$). ^{13}C NMR (100 MHz, DMSO; 100 MHz, CD_3SO): δ 170.3, 166.0, 154.5, 143.6, 142.4, 136.1, 133.5, 131.2, 131.0, 128.8, 127.5, 127.0, 127.0, δ126.7, 126.6, 126.6, 125.3, 121.0, 118.7, 113.5, 110.0, 79.9, 28.7, 13.2, 10.9. Retention time: 5.10 min (HPLC C-18 column, acetonitrile/DMGA (5 mM, pH 7.4) = 80:20 (v:v), flow rate 1.0 mL/min). HR-ESIMS: m/z calcd for $C_{32}H_{37}N_5O_6SCl^+$ ($M + H^+$) 654.214 76, found 654.214 99; m/z calcd for $C_{32}H_{37}N_5O_6SCl^+$ ($M + Na^+$) 676.196 70, found 676.196 97.

4.11. Synthesis of 3-[3,5-Dimethyl-4-(piperazine-1-carbonyl)-1*H*-pyrrol-2-ylmethylene]-2-oxo-2,3-dihyro-1*H*-indole-5-sulfonic Acid (3-Chlorophenyl)methylamide Hydrochloride (13). 4-(5-{5-[3-Chlorophenyl)methylsulfomyl]-2-oxo-dihydroindol-3-yllidenemethyl}-2,4-dimethyl-1*H*-pyrrole-3-carbonyl)piperazine-1-carboxylic acid *tert*-butyl ester (**12**, 150 mg, 0.22 mmol) was suspended in 5 mL of ethyl acetate, and 5 mL of hydrochloric acid/ethyl acetate (4 M) was added at ice-cold temperature. After the solution was allowed to stand for 1 h at room temperature, the solvent was evaporated under vacuum, yielding 3-[3,5-dimethyl-4-(piperazine-1-carbonyl)-1*H*-pyrrol-2-ylmethylene]-2-oxo-2,3-dihyro-1*H*-indole-5-sulfonic acid (3-chlorophenyl)methylamide hydrochloride (**13**) as a yellow solid (100 mg, 74%). ^{1}H NMR (400 MHz, DMSO-d_6) 2.30, 2.43 (2 × s, 2 × 3H, 2 × CH_3); 3.18 (s, 3H, CH_3); 3.40 (m, 8H, piperazyl-H); 7.00−7.70 (m, 7H, aromatic-H and 1H, olefinic-H). ^{13}C NMR (100 MHz, DMSO-d_6) 3.08 (s, 3H, CH_3); 3.53 (s, 2H, CH_2); 6.92−7.16 (m, 7H, H-aromatic); 10.89 (br, s, NH). HR-ESIMS: m/z calcd for $C_{27}H_{29}N_5O_4SCl^+$ (M − Cl), 554.16233; found 554.16248. Retention time: 6.08 min (HPLC C-18 column, acetonitrile/DMGA (5 mM, pH 7.4) = 80:20 (v:v)).

4.12. Radiosynthesis of [^{11}C]14. The cyclotron-made [^{11}C]carbon dioxide was converted to [^{11}C]methyl iodide by reduction with lithium aluminum hydride and hydroiodide.[43] The labeled methyl iodide [^{11}C]CH_3I was concurrently distilled and trapped in a dry 5 mL conical reaction vial cooled in an ice bath which was previously filled with a solution of 2 mg of **13** and 10 mg of potassium carbonate dissolved in 0.3 mL dimethylformamide. Trapping of [^{11}C]methyl iodide was monitored by measuring the activity in the isotope calibrator until the maximal value was attained. The reaction mixture was sealed and heated at 140 °C for 10 min in a heating block, cooled to room temperature, and diluted with water. The radiolabeled reaction mixture was passed through a Waters C-18 Sep-Pak cartridge previous conditioned with ethanol and then water to remove the nonorganic impurities. The Sep-Pak cartridge was washed with 10 mL of water and dried with a rapid air bolus, and the radiolabeled product was eluted with ethanol, loaded onto a preparative HPLC (Luna 5 μm C18 250mm × 10 mm) column, and eluted with acetonitrile and water (flow rate 3 mL/min (8:2 v/v)). The retention time was 6.08 min (HPLC C-18 column, acetonitrile/DMGA (5 mM, pH 7.4) = 80:20 (v:v)). The radiochemical purity of [^{11}C]**14** was >95% as determined by radio-HPLC, and the total synthesis time was 30−40 min from the end of bombardment (EOB).

4.13. Lung Cancer Cell Culture and in Vivo Nude Mouse Xenograft Model. Lung cancer xenografts with NCI-H520 and NCI-H1975 lung adenocarcinoma cells were established for this imaging study. Both the NCI-H520 and NCI-H1975 cell lines were obtained from American Type Culture Collection (ATCC, Manassas, VA) and grown in RPMI-1640 media (Hyclone, Logan, UT) supplemented with 10% (v/v) fetal bovine serum under standard cell culture conditions. Six-week-old female Ncr-nu (Nude) mice were purchased from Charles River Laboratories (Wilmington, MA) and hosted in the pathogen-free animal facility at Case Western Reserve University. In vivo animal studies were performed according to institution-approved protocols and guidelines. Xenografts of the NCI-H1975 and NCI-H520 lung cancer cells were established by intradermally injecting 3×10^6 viable cells in RPMI 1640 media into the flank/leg region of nude mice to produce subcutaneous tumors.[42] Body weight was recorded for each animal twice weekly to monitor potential toxicities. Tumor xenografts were subsequently dissected and harvested at the end of the experiments after completion of the imaging studies and formalin-fixed and stained with hematoxylin and eosin (H&E) using standard techniques.

4.14. Micro-PET/MRI imaging. A pair of xenograft model mice was placed on a plastic bed that was suitable for both PET and MRI scanning following anesthesia with 2.0% isoflurane delivered in oxygen gas with a nosecone. The micro-PET experiment was performed on a Concord R4 micro-PET scanner (Siemens Medical Solutions, Knoxville, TN). Transmission scans were acquired for 10 min by using a ^{57}Co source

which was subsequently used for attenuation correction. [^{11}C]**14** (18.5 MBq) was then injected into the tail vein. The image acquisition started immediately after the injection. The dynamic imaging was collected for 90 min in a list mode. PET images were reconstructed into a 128 × 128 matrix with 0.8 mm slice thickness. Twelve frames were acquired within the scan duration starting from 10 min (frames 0−5) to 5 min (6−11) during the experiment.

Following micro-PET imaging, the animals were immediately transferred to a Bruker Biospec 9.4 T MRI scanner under anesthesia to produce high resolution images as roadmaps for micro-PET imaging. The entire animal bed was moved to minimize movement of the animals between the MRI and PET scans. After initial localization scans, the two mice were simultaneously scanned using T2-weighted imaging. Each animal's respiration rate was monitored, and the animal's core body temperature was also maintained at 37 ± 2 °C throughout the scanning procedure. High-resolution anatomic MR images of the tumor region were acquired using contiguous multislice 2D spin echo and 3D gradient echo techniques.

4.15. Quantitative Image Analysis. Following micro-PET and MRI imaging, we conducted quantitative image analysis in order to evaluate the in vivo pharmacokinetic profiles of [^{11}C]**14** in xenograft tumor tissues. The micro-PET images were registered with MR images to ensure the consistency of the anatomical localization of [^{11}C]**14** in tumor tissue. Volumes of interest (VOI) of the xenografts were then defined and delineated in 3D on MR images. The coregistered images were used for quantitative image analysis to determine [^{11}C]**14** uptake and retention associated with tumor tissues. To generate a radioactivity versus time curve, the mean radioactivity in the VOI was calculated, corrected for ^{11}C decay, plotted, and expressed in terms of standard uptake volume [(μCi/cm^3)/(μCi/g)] as a function of time.

4.16. Ex Vivo Bioassay of MET Expression. For the in vitro cellular protein expression analysis, the lung cancer cell lines were cultured under regular growth conditions to exponential growth phase. Cellular proteins were extracted from whole cells as previously described.[16] Immunoblotting was performed as previously described[16,44] using the following primary antibodies as indicated: p-MET [Y1234/1235] (Cell Signaling Technology, Danvers, MA), MET (C-12, Santa Cruz Biotechnology, Santa Cruz, CA), p-EGFR[Y1068] (Cell Signaling), EGFR (Santa Cruz Biotechnology), and actin (Santa Cruz Biotechnology). Following MRI and micro-PET studies, the animals bearing the lung cancer xenografts were sacrificed in accordance with institutional guidelines, and the xenograft tumors were dissected and harvested under standard techniques. The xenografts were then formalin-fixed in 5% formalin for 16 h, processed for hematoxylin and eosin (H&E) staining as well as immunohistochemical staining using rabbit polyclonal primary antibody against total MET (C-12, Santa Cruz Biotechnology) at 1:100 dilution as previously described.[16] Isotype matched rabbit IgG was used as negative control treatment as well. The immunohistochemistry was performed using the Tissue Procurement and Histology Core Facility of the Case Comprehensive Cancer Center.

Acknowledgment. We thank Dr. George Bakale for proofreading the manuscript. This work is supported by Case Center for Imaging Research and Case Comprehensive Cancer Center. P.C.M. is supported by NIH/National Cancer Institute—K08 Mentored Clinical Scientist Career Development Award (Grant 5K08CA102545-04) and the Sol Siegal Lung Cancer Research in Honor of Molly Siegal Grant Program.

Supporting Information Available: Table listing the analytical data for compounds **7**−**13**; spectra of HPLC, HRMS, ^{1}HNMR, and ^{13}C NMR. This material is available free of charge via the Internet at http://pubs.acs.org.

References

(1) Sun, S.; Schiller, J. H.; Spinola, M.; Minna, J. D. New molecularly targeted therapies for lung cancer. *J. Clin. Invest.* **2007**, *117*, 2740–2750.
(2) Savage, D. G.; Antman, K. H. Imatinib mesylate—a new oral targeted therapy. *N. Engl. J. Med.* **2002**, *346*, 683–693.
(3) Ryan, Q.; Ibrahim, A.; Cohen, M. H.; Johnson, J.; Ko, C. W.; Sridhara, R.; Justice, R.; Pazdur, R. FDA drug approval summary: lapatinib in combination with capecitabine for previously treated metastatic breast cancer that overexpresses HER-2. *Oncologist* **2008**, *13*, 1114–1119.
(4) Goodman, V. L.; Rock, E. P.; Dagher, R.; Ramchandani, R. P.; Abraham, S.; Gobburu, J. V.; Booth, B. P.; Verbois, S. L.; Morse, D. E.; Liang, C. Y.; Chidambaram, N.; Jiang, J. X.; Tang, S.; Mahjoob, K.; Justice, R.; Pazdur, R. Approval summary: sunitinib for the treatment of imatinib refractory or intolerant gastrointestinal stromal tumors and advanced renal cell carcinoma. *Clin. Cancer Res.* **2007**, *13*, 1367–1373.
(5) Wilhelm, S.; Carter, C.; Lynch, M.; Lowinger, T.; Dumas, J.; Smith, R. A.; Schwartz, B.; Simantov, R.; Kelley, S. Discovery and development of sorafenib: a multikinase inhibitor for treating cancer. *Nat. Rev. Drug Discovery* **2006**, *5*, 835–844.
(6) Birchmeier, C.; Birchmeier, W.; Gherardi, E.; Vande Woude, G. F. Met, metastasis, motility and more. *Nat. Rev. Mol. Cell Biol.* **2003**, *4*, 915–925.
(7) Ma, P. C.; Maulik, G.; Christensen, J.; Salgia, R. c-Met: structure, functions and potential for therapeutic inhibition. *Cancer Metastasis Rev* **2003**, *22*, 309–325.
(8) Birchmeier, C.; Gherardi, E. Developmental roles of HGF/SF and its receptor, the c-Met tyrosine kinase. *Trends Cell Biol* **1998**, *8*, 404–410.
(9) Rosario, M.; Birchmeier, W. How to make tubes: signaling by the Met receptor tyrosine kinase. *Trends Cell Biol* **2003**, *13*, 328–335.
(10) Dietrich, S.; Uppalapati, R.; Seiwert, T. Y.; Ma, P. C. Role of c-MET in upper aerodigestive malignancies—from biology to novel therapies. *J. Environ. Pathol., Toxicol. Oncol.* **2005**, *24*, 149–162.
(11) Sattler, M.; Pride, Y. B.; Ma, P.; Gramlich, J. L.; Chu, S. C.; Quinnan, L. A.; Shirazian, S.; Liang, C.; Podar, K.; Christensen, J. G.; Salgia, R. A novel small molecule met inhibitor induces apoptosis in cells transformed by the oncogenic TPR-MET tyrosine kinase. *Cancer Res.* **2003**, *63*, 5462–5469.
(12) Corso, S.; Comoglio, P. M.; Giordano, S. Cancer therapy: can the challenge be MET? *Trends Mol. Med.* **2005**, *11*, 284–292.
(13) Eder, J. P.; Vande Woude, G. F.; Boerner, S. A.; LoRusso, P. M. Novel therapeutic inhibitors of the c-Met signaling pathway in cancer. *Clin. Cancer Res.* **2009**, *15*, 2207–2214.
(14) Knudsen, B. S.; Vande Woude, G. Showering c-MET-dependent cancers with drugs. *Curr. Opin. Genet. Dev.* **2008**, *18*, 87–96.
(15) Ma, P. C.; Tretiakova, M. S.; Nallasura, V.; Jagadeeswaran, R.; Husain, A. N.; Salgia, R. Downstream signalling and specific inhibition of c-MET/HGF pathway in small cell lung cancer: implications for tumour invasion. *Br. J. Cancer* **2007**, *97*, 368–377.
(16) Ma, P. C.; Jagadeeswaran, R.; Jagadeesh, S.; Tretiakova, M. S.; Nallasura, V.; Fox, E. A.; Hansen, M.; Schaefer, E.; Naoki, K.; Lader, A.; Richards, W.; Sugarbaker, D.; Husain, A. N.; Christensen, J. G.; Salgia, R. Functional expression and mutations of c-Met and its therapeutic inhibition with SU11274 and small interfering RNA in non-small cell lung cancer. *Cancer Res.* **2005**, *65*, 1479–1488.
(17) Ma, P. C.; Schaefer, E.; Christensen, J. G.; Salgia, R. A selective small molecule c-MET inhibitor, PHA665752, cooperates with rapamycin. *Clin. Cancer Res.* **2005**, *11*, 2312–2319.
(18) Shaharabany, M.; Abramovitch, R.; Kushnir, T.; Tsarfaty, G.; Ravid-Megido, M.; Horev, J.; Ron, R.; Itzchak, Y.; Tsarfaty, I. In vivo molecular imaging of met tyrosine kinase growth factor receptor activity in normal organs and breast tumors. *Cancer Res.* **2001**, *61*, 4873–4878.
(19) Tsarfaty, G.; Stein, G. Y.; Moshitch-Moshkovitz, S.; Kaufman, D. W.; Cao, B.; Resau, J. H.; Vande Woude, G. F.; Tsarfaty, I. HGF/SF increases tumor blood volume: a novel tool for the in vivo functional molecular imaging of Met. *Neoplasia* **2006**, *8*, 344–352.
(20) Towner, R. A.; Smith, N.; Tesiram, Y. A.; Abbott, A.; Saunders, D.; Blindauer, R.; Herlea, O.; Silasi-Mansat, R.; Lupu, F. In vivo detection of c-MET expression in a rat hepatocarcinogenesis model using molecularly targeted magnetic resonance imaging. *Mol. Imaging* **2007**, *6*, 18–29.

(21) Perk, L. R.; Stigter-van Walsum, M.; Visser, G. W.; Kloet, R. W.; Vosjan, M. J.; Leemans, C. R.; Giaccone, G.; Albano, R.; Comoglio, P. M.; van Dongen, G. A. Quantitative PET imaging of Met-expressing human cancer xenografts with ^{89}Zr-labelled monoclonal antibody DN30. *Eur. J. Nucl. Med. Mol. Imaging* **2008**, *35*, 1857–1867.
(22) Hay, R. V.; Cao, B.; Skinner, R. S.; Su, Y.; Zhao, P.; Gustafson, M. F.; Qian, C. N.; Teh, B. T.; Knudsen, B. S.; Resau, J. H.; Shen, S.; Waters, D. J.; Gross, M. D.; Vande Woude, G. F. Nuclear imaging of Met-expressing human and canine cancer xenografts with radiolabeled monoclonal antibodies (MetSeek). *Clin. Cancer Res.* **2005**, *11*, 7064s–7069s.
(23) Schroeder, G. M.; An, Y.; Cai, Z. W.; Chen, X. T.; Clark, C.; Cornelius, L. A.; Dai, J.; Gullo-Brown, J.; Gupta, A.; Henley, B.; Hunt, J. T.; Jeyaseelan, R.; Kamath, A.; Kim, K.; Lippy, J.; Lombardo, L. J.; Manne, V.; Oppenheimer, S.; Sack, J. S.; Schmidt, R. J.; Shen, G.; Stefanski, K.; Tokarski, J. S.; Trainor, G. L.; Wautlet, B. S.; Wei, D.; Williams, D. K.; Zhang, Y.; Fargnoli, J.; Borzilleri, R. M. Discovery of *N*-(4-(2-amino-3-chloropyridin-4-yloxy)-3-fluorophenyl)-4-ethoxy-1-(4-fluorophenyl)-2-oxo-1,2-dihydropyridine-3-carboxamide (BMS-777607), a selective and orally efficacious inhibitor of the Met kinase superfamily. *J. Med. Chem.* **2009**, *52*, 1251–1254.
(24) Zhang, Y.; Kaplan-Lefko, P. J.; Rex, K.; Yang, Y.; Moriguchi, J.; Osgood, T.; Mattson, B.; Coxon, A.; Reese, M.; Kim, T. S.; Lin, J.; Chen, A.; Burgess, T. L.; Dussault, I. Identification of a novel recepteur d'origine nantais/c-met small-molecule kinase inhibitor with antitumor activity in vivo. *Cancer Res.* **2008**, *68*, 6680–6687.
(25) Liu, L.; Siegmund, A.; Xi, N.; Kaplan-Lefko, P.; Rex, K.; Chen, A.; Lin, J.; Moriguchi, J.; Berry, L.; Huang, L.; Teffera, Y.; Yang, Y.; Zhang, Y.; Bellon, S. F.; Lee, M.; Shimanovich, R.; Bak, A.; Dominguez, C.; Norman, M. H.; Harmange, J. C.; Dussault, I.; Kim, T. S. Discovery of a potent, selective, and orally bioavailable c-Met inhibitor: 1-(2-hydroxy-2-methylpropyl)-*N*-(5-(7-methoxyquinolin-4-yloxy)pyridin-2-yl)-5-methyl-3-oxo-2-phenyl-2,3-dihydro-1*H*-pyrazole-4-carboxamide (AMG 458). *J. Med. Chem.* **2008**, *51*, 3688–3691.
(26) Yang, Y.; Wislez, M.; Fujimoto, N.; Prudkin, L.; Izzo, J. G.; Uno, F.; Ji, L.; Hanna, A. E.; Langley, R. R.; Liu, D.; Johnson, F. M.; Wistuba, I.; Kurie, J. M. A selective small molecule inhibitor of c-Met, PHA-665752, reverses lung premalignancy induced by mutant K-ras. *Mol. Cancer Ther.* **2008**, *7*, 952–960.
(27) Chattopadhyay, C.; El-Naggar, A. K.; Williams, M. D.; Clayman, G. L. Small molecule c-MET inhibitor PHA665752: effect on cell growth and motility in papillary thyroid carcinoma. *Head Neck* **2008**, *30*, 991–1000.
(28) Tseng, J. R.; Kang, K. W.; Dandekar, M.; Yaghoubi, S.; Lee, J. H.; Christensen, J. G.; Muir, S.; Vincent, P. W.; Michaud, N. R.; Gambhir, S. S. Preclinical efficacy of the c-Met inhibitor CE-355621 in a U87 MG mouse xenograft model evaluated by 18F-FDG small-animal PET. *J. Nucl. Med.* **2008**, *49*, 129–134.
(29) Koon, E. C.; Ma, P. C.; Salgia, R.; Welch, W. R.; Christensen, J. G.; Berkowitz, R. S.; Mok, S. C. Effect of a c-Met-specific, ATP-competitive small-molecule inhibitor SU11274 on human ovarian carcinoma cell growth, motility, and invasion. *Int. J. Gynecol. Cancer* **2008**, *18*, 976–984.
(30) Zou, H. Y.; Li, Q.; Lee, J. H.; Arango, M. E.; McDonnell, S. R.; Yamazaki, S.; Koudriakova, T. B.; Alton, G.; Cui, J. J.; Kung, P. P.; Nambu, M. D.; Los, G.; Bender, S. L.; Mroczkowski, B.; Christensen, J. G. An orally available small-molecule inhibitor of c-Met, PF-2341066, exhibits cytoreductive antitumor efficacy through antiproliferative and antiangiogenic mechanisms. *Cancer Res.* **2007**, *67*, 4408–4417.
(31) Puri, N.; Khramtsov, A.; Ahmed, S.; Nallasura, V.; Hetzel, J. T.; Jagadeeswaran, R.; Karczmar, G.; Salgia, R. A selective small molecule inhibitor of c-Met, PHA665752, inhibits tumorigenicity and angiogenesis in mouse lung cancer xenografts. *Cancer Res.* **2007**, *67*, 3529–3534.
(32) Smolen, G. A.; Sordella, R.; Muir, B.; Mohapatra, G.; Barmettler, A.; Archibald, H.; Kim, W. J.; Okimoto, R. A.; Bell, D. W.; Sgroi, D. C.; Christensen, J. G.; Settleman, J.; Haber, D. A. Amplification of MET may identify a subset of cancers with extreme sensitivity to the selective tyrosine kinase inhibitor PHA-665752. *Proc. Natl. Acad. Sci. U.S.A.* **2006**, *103*, 2316–2321.
(33) Wang, S. Y.; Chen, B.; Zhan, Y. Q.; Xu, W. X.; Li, C. Y.; Yang, R. F.; Zheng, H.; Yue, P. B.; Larsen, S. H.; Sun, H. B.; Yang, X. SU5416 is a potent inhibitor of hepatocyte growth factor receptor (c-Met) and blocks HGF-induced invasiveness of human HepG2 hepatoma cells. *J. Hepatol.* **2004**, *41*, 267–273.
(34) Christensen, J. G.; Schreck, R.; Burrows, J.; Kuruganti, P.; Chan, E.; Le, P.; Chen, J.; Wang, X.; Ruslim, L.; Blake, R.; Lipson, K. E.; Ramphal, J.; Do, S.; Cui, J. J.; Cherrington, J. M.; Mendel, D. B. A selective small molecule inhibitor of c-Met kinase inhibits c-Met-dependent phenotypes in vitro and exhibits cytoreductive antitumor activity in vivo. *Cancer Res.* **2003**, *63*, 7345–7355.
(35) Christensen, J. G.; Burrows, J.; Salgia, R. c-Met as a target for human cancer and characterization of inhibitors for therapeutic intervention. *Cancer Lett.* **2005**, *225*, 1–26.
(36) Kopka, K.; Faust, A.; Keul, P.; Wagner, S.; Breyholz, H. J.; Holtke, C.; Schober, O.; Schafers, M.; Levkau, B. 5-Pyrrolidinylsulfonyl isatins as a potential tool for the molecular imaging of caspases in apoptosis. *J. Med. Chem.* **2006**, *49*, 6704–6715.
(37) Li, H. H.; Zheng, X. H.; Tan, J. Z.; Chen, L. L.; Liu, H.; Luo, X. M.; Shen, X.; Lin, L. P.; Chen, K. X.; Ding, J.; Jiang, H. L. Design, synthesis, antitumor evaluations and molecular modeling studies of novel 3,5-substituted indolin-2-one derivatives. *Acta Pharmacol. Sin.* **2007**, *28*, 140–152.
(38) Sun, L.; Liang, C.; Shirazian, S.; Zhou, Y.; Miller, T.; Cui, J.; Fukuda, J. Y.; Chu, J. Y.; Nematalla, A.; Wang, X.; Chen, H.; Sistla, A.; Luu, T. C.; Tang, F.; Wei, J.; Tang, C. Discovery of 5-[5-fluoro-2-oxo-1,2- dihydroindol-(3*Z*)-ylidenemethyl]-2,4- dimethyl-1*H*-pyrrole-3-carboxylic acid (2-diethylaminoethyl)amide, a novel tyrosine kinase inhibitor targeting vascular endothelial and platelet-derived growth factor receptor tyrosine kinase. *J. Med. Chem.* **2003**, *46*, 1116–1119.
(39) Bell, I. M.; Stirdivant, S. M.; Ahern, J.; Culberson, J. C.; Darke, P. L.; Dinsmore, C. J.; Drakas, R. A.; Gallicchio, S. N.; Graham, S. L.; Heimbrook, D. C.; Hall, D. L.; Hua, J.; Kett, N. R.; Kim, A. S.; Kornienko, M.; Kuo, L. C.; Munshi, S. K.; Quigley, A. G.; Reid, J. C.; Trotter, B. W.; Waxman, L. H.; Williams, T. M.; Zartman, C. B. Biochemical and structural characterization of a novel class of inhibitors of the type 1 insulin-like growth factor and insulin receptor kinases. *Biochemistry* **2005**, *44*, 9430–9440.
(40) Manley, J. M.; Kalman, M. J.; Conway, B. G.; Ball, C. C.; Havens, J. L.; Vaidyanathan, R. Early amidation approach to 3-[(4-amido)pyrrol-2-yl]-2-indolinones. *J. Org. Chem.* **2003**, *68*, 6447–6450.
(41) Sun, L.; Cui, J.; Liang, C.; Zhou, Y.; Nematalla, A.; Wang, X.; Chen, H.; Tang, C.; Wei, J. Rational design of 4,5-disubstituted-5,7-dihydro-pyrrolo[2,3-*d*]pyrimidin-6-ones as a novel class of inhibitors of epidermal growth factor receptor (EGF-R) and Her2-(p185(erbB)) tyrosine kinases. *Bioorg. Med. Chem. Lett.* **2002**, *12*, 2153–2157.
(42) Tang, Z.; Du, R.; Jiang, S.; Wu, C.; Barkauskas, D. S.; Richey, J.; Molter, J.; Lam, M.; Flask, C.; Gerson, S.; Dowlati, A.; Liu, L.; Lee, Z.; Halmos, B.; Wang, Y.; Kern, J. A.; Ma, P. C. Dual MET-EGFR combinatorial inhibition against T790M-EGFR-mediated erlotinib-resistant lung cancer. *Br. J. Cancer* **2008**, *99*, 911–922.
(43) Langstrom, B.; Lundqvist, H. The preparation of ^{11}C-methyl iodide and its use in the synthesis of ^{11}C-methyl-L-methionine. *Int. J. Appl. Radiat. Isot.* **1976**, *27*, 357–363.
(44) Ma, P. C.; Tretiakova, M. S.; MacKinnon, A. C.; Ramnath, N.; Johnson, C.; Dietrich, S.; Seiwert, T.; Christensen, J. G.; Jagadeeswaran, R.; Krausz, T.; Vokes, E. E.; Husain, A. N.; Salgia, R. Expression and mutational analysis of MET in human solid cancers. *Genes, Chromosomes Cancer* **2008**, *47*, 1025–1037.